PAN
ARCHIVES OF ACOUSTICS
Vol. **44**, No. 4, pp. 807–813 (2019)
DOI: 10.24425/aoa.2019.129735

Technical Note

Acoustic Emission Response and Damage Process for Q235 Steel in an *in Situ* Tensile Test

Ying ZHANG[(2)], Yue LI[(3)], Huan Sheng LAI[(1)*], Chunmei BAI[(4)], Kang Lin LIU[(5)]

[(1)] *Sino-French Institute of Nuclear Engineering and Technology*
Sun Yat-sen University
Zhuhai 519082, China
[*] Corresponding Author e-mail: sheng158@hotmail.com

[(2)] *School of Environmental & Safety Engineering*
Changzhou University
Changzhou 213164, China

[(3)] *Northeast Petroleum University*
Daqing 163000, China

[(4)] *School of Civil Engineering*
Sun Yat-sen University
Zhuhai 519082, China

[(5)] *School of Chemical Engineering*
Fuzhou University
Fuzhou, 350-116, China

(*received March 15, 2019; accepted September 27, 2019*)

Q235 steel is widely used in engineering and construction. Therefore, it is important to identify the damage mechanism and the acoustic emission (AE) response of the material to ensure the safety of structures. In this study, an AE monitor system and an in situ tensile test with an optical microscope were used to investigate the AE response and insight into the damage process of Q235 steel. The surface of the specimen was polished and etched before the test in order to improve the quality of micrographs. Two kinds of AE responses, namely a burst and a continuous signal, were recorded by the AE monitor system during the test. Based on the in situ test, it was observed that the damage of Q235 steel was induced by the crystal slip and the inclusion fracture. Since the crystal slip was an ongoing process, continuous AE signals were produced, while burst AE signals were possibly produced by the inclusion fracture which occurred suddenly with released higher energy. In addition, a great number of AE signals with high amplitude were observed during the yielding stage and then the number and amplitude decreased.

Keywords: Q235; damage; acoustic emission; *in situ* tensile test.

1. Introduction

Q235 steel is widely used in engineering and construction because of the good comprehensive properties. Therefore, it is important to understand the damage evolution of Q235 steel in details to ensure the safety and structural integral. The acoustic emission (AE) method is a nondestructive technique that can detect certain damages in real time and on-line (Haidar *et al.*, 2005; Ito, Enoki, 2007; Casiez *et al.*, 2014). It is one of the extensively used method in structural health management (Lugo *et al.*, 2011; Rabiei, Modarres, 2013). AE signals are generated from material damages such as twining, dislocation, cavitation, and crystal slip (Heiple, Carpenter, 1987; Bohlen *et al.*, 2004; Trojanová *et al.*, 2010). Previous work has shown that the damage response of Q235B steel can be assessed by the AE method (Zhang *et al.*, 2015) and the defects can be located accurately (Wu *et al.*, 2008; Jiang, Xu, 2012).

Even though the AE method can detect the damage in the material, it cannot observe the damaging process directly nor identify the damage mechanism when used alone. An effective way to study the damage mechanism is to directly observe the damaging process. An *in situ* test coupled to optical microscopy (Li *et al.*, 2016), synchrotron X-ray tomography (Mire *et al.*, 2007), or scanning electron microscopy (Shao *et al.*, 2013; Chen *et al.*, 2014; Zhang *et al.*, 2017; 2018) is an efficient way to directly observe the damaging process. However, limited *in situ* studies have been carried out on Q235 steel with the AE method.

The goal of this work is to clarify the mechanism of the damaging process using the corresponding AE signals in Q235 steel. First, an *in situ* tensile test system was set-up to monitor AE signals and coupled with optical microscopy using a CCD camera to continuously visualize the damage evolution in real time and online. Then, the damage evolution were analyzed based on the AE signals and optical micrographs.

2. Experimental details

The experimental setup for the *in situ* tensile test is shown in Fig. 1. It was composed of an AE monitor system PCI-2, an *in situ* tensile testing machine SEMtester100, and an optical microscope MZ1000 with a CCD camera. The dimensions of the test bench were $173 \times 120 \times 19$ mm so that it could be placed on the stage of the optical microscope. Therefore, the damage progress and the AE signals could be recorded in real time and on-line during the test. The parameter setting and the data analysis were performed by the data acquisition system (Fig. 1). The AE signals were recorded by a micro sensor (Fig. 1) with a size of 5×4 mm and a frequency ranging from 200 to 750 kHz. The AE signals were transmitted through a 2/4/6-AST preamplifier and then received by the PCI-2 AE instrument. The detailed specifications are given in Table 1.

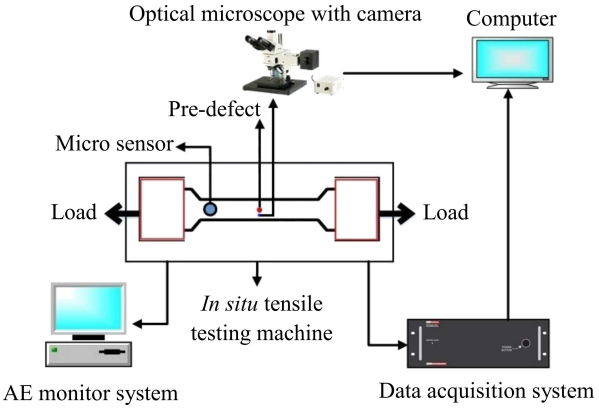

Fig. 1. Experimental setup.

The specimen was made of Q235 steel with a total length of 50 mm and a thickness of 0.5 mm, as shown in Fig. 2. A small hole with a diameter of 0.1 mm was made in the middle of the specimen to trigger failure at this location (Li *et al.*, 2016) and the optical microscope was used to record images around that hole, as shown in Fig. 1. The surface of the specimen was polished and etched in a 4% (V/V) solution of nitric acid and alcohol for about 20 s to be able to observe the Q235 steel sample. The tensile rate was 0.1 mm/min and the image was magnified 500 times by the optical microscope. The AE signals and the images were automatically recorded simultaneously until the specimen fractured. Three specimens were tested in this study.

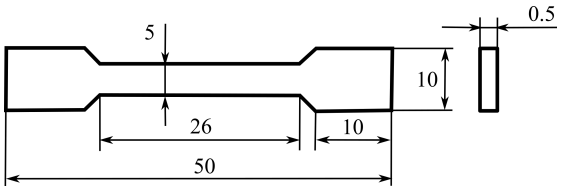

Fig. 2. Dimensions of the tensile test specimen.

3. Results and discussions

3.1. AE signal analysis

The typical experimental temporal evolution of the stress and AE signal amplitudes are shown in Fig. 3. There are approximately four stages. The first stage,

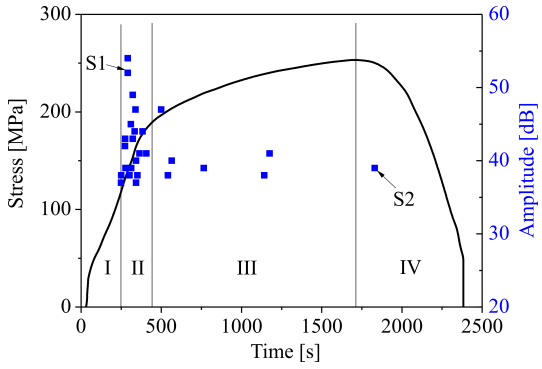

Fig. 3. Temporal stress and amplitude evolution of the AE signals.

Table 1. Specifications of the AE monitoring system.

Threshold [dB]	Sampling rate [MHz]	Sampling length [k]	Gain [dB]	Peak definition time [μs]	Hit definition time [μs]	Hit lock time [μs]
33	1	2	40	300	600	600

from 0 to 248 s, was the elastic phase. A great number of AE signals could be detected at this stage but they were noise and filtered by the threshold of 33 dB. The reason was that the AE signal was generated by the energy released through dislocation, crystal slip, and inclusion fracture (Haidar *et al.*, 2005; Ito, Enoki, 2007; Casiez *et al.*, 2014), but the AE signal could not be produced at elastic phase, because the elastic deformation could be totally recovered and no energy was released. Therefore, no AE signal was detected at this stage. This also means that no damage occurred in the elastic phase. The yield stage occurred from 249 to 429 s, where several signals of high amplitude were observed. This means that the damage or yield deformation was very significant and that a large amount of energy was released rapidly. The hardening stage took place from 430 to 1736 s. The number and amplitude of the AE signals decreased in this stage. This could be due to the increase in the resistance of the dislocation or during the crystal slip with their density. Therefore, the damage through dislocation or crystal slip decreased, which led to a decrease in AE signals in this stage. The final stage of necking-fracture was from 1737 to 2198 s. There was only one AE signal at the initial point of necking and no difference was found in the amplitude of the AE signal between the hardening and necking-fracture stages. Therefore, the number and amplitude of the AE signals reached their maximum values in the yield stage but it was impossible to distinguish between the hardening and the necking-fracture stage using the amplitude of AE signals.

Two types of AE signals were generated during the test. The first type was a burst signal, as shown in Fig. 4. It appeared after 291 s, which is noted at S1 in Fig. 3. The signal increased rapidly and lasted for a long time, as shown in Fig. 4a. The amplitude was 52 dB, the ringing count was 69, and the center frequency was 271 KHz. The time-frequency distribution is shown in Fig. 4c. The high-energy state lasted for a very short time and then decayed rapidly. The second type of AE signals was a continuous signal, as shown in Fig. 5a. It appeared after 1831 s, which is noted as S2 in Fig. 3. The amplitude (40 dB), ringing count (2), and center frequency (210 kHz) were smaller than for the burst signal at S1. Continuous signals were also observed for Q235 steel, 304 steel and brass (H62) under a tensile test (Su *et al.*, 2018). When comparing Fig. 4b and Fig. 5b, the magnitude of the continuous signal was much smaller than the burst signal. The time-frequency distribution was not obvious for the continuous signal, as shown in Fig. 5c. The characteristic parameters of all AE signals are listed in Table 2. As shown Table 2 it could be found that there were more burst AE signals with high energy in the yield stage.

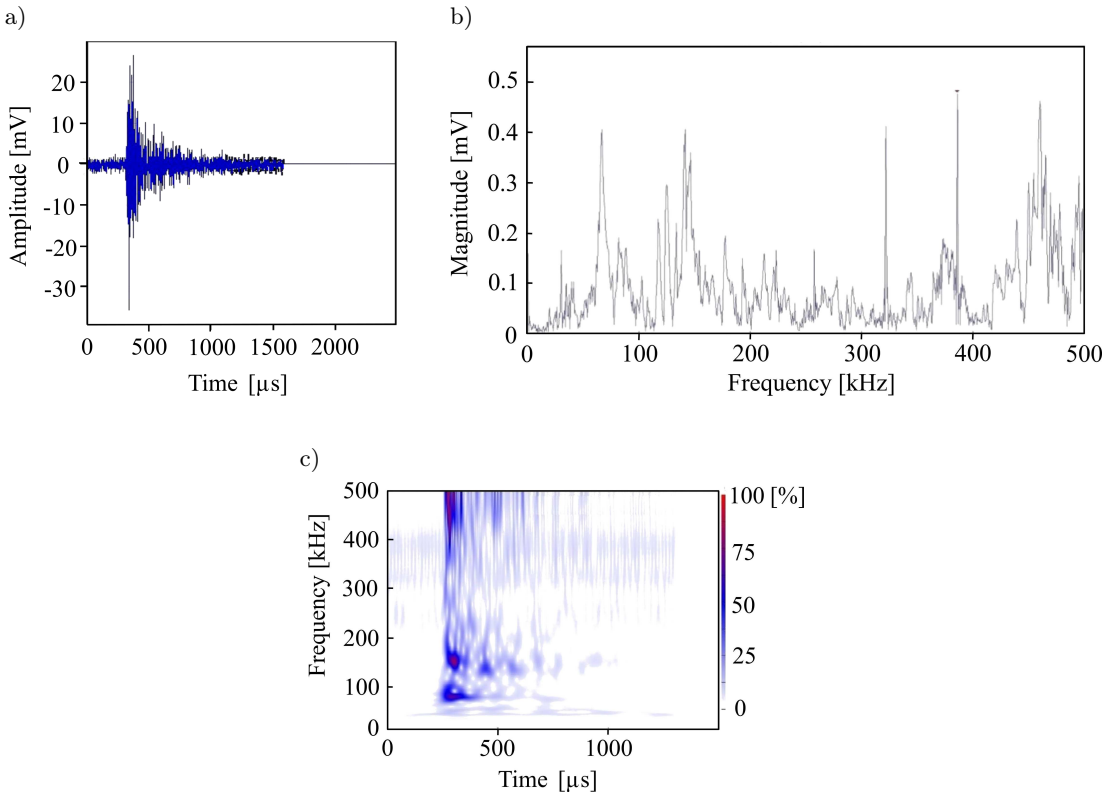

Fig. 4. Burst signal at 291 s for the S1 point: a) voltage evolution of the burst signals, b) fast Fourier transformation (FFT) of signal shown in Fig. 4a, c) continuous wavelet transformation (CWT) of signal shown in Fig. 4a.

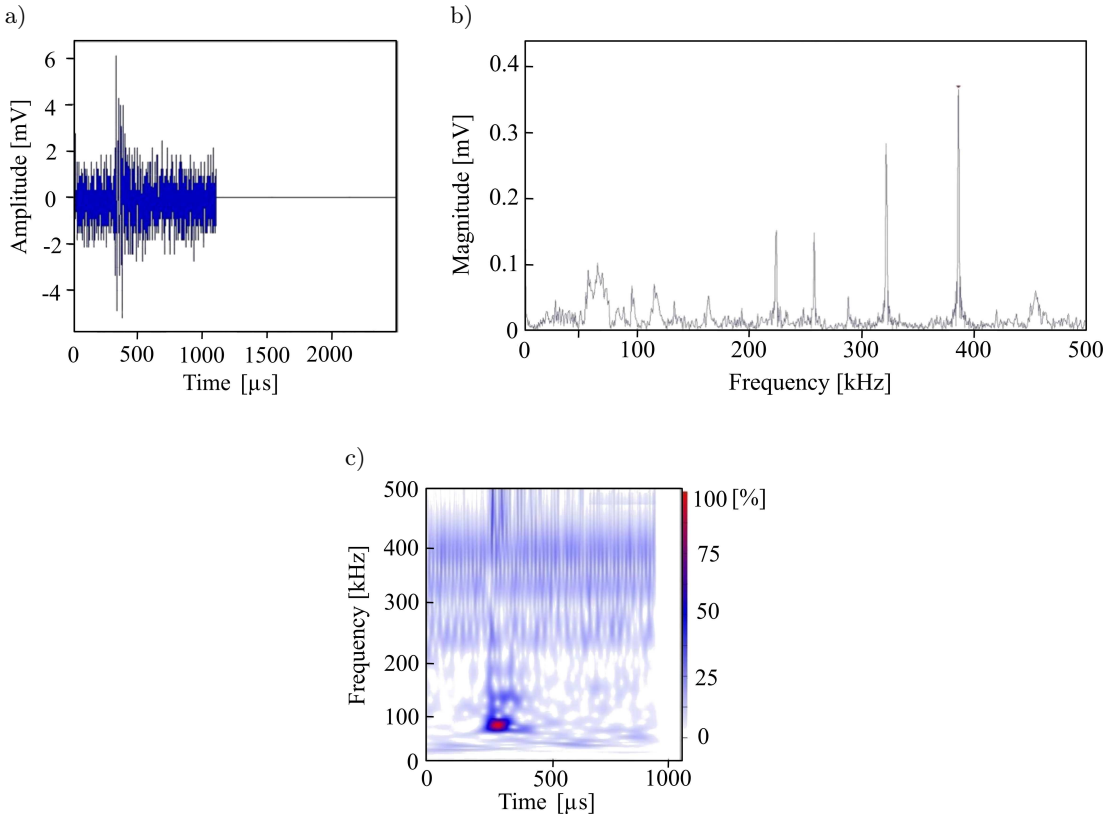

Fig. 5. Continuous signal at 1831 s for the S2 point: a) voltage evolution of the continuous signal, b) fast Fourier transformation (FFT) of signal shown in Fig. 5a, c) continuous wavelet transformation (CWT) of signal shown in Fig. 5a.

Table 2. Characteristics of the AE signals observed.

Signal type	Number of signals	Generation stage	Amplitude [dB]	Ringing count	Center frequency [kHz]
Burst	11	9 at yield stage, 2 after yield stage	41–49	14–38	244–286
Continuous	11	6 at yield stage, 5 after yield stage	36–44	2–11	208–263

3.2. Optical microscopy analysis

The observations from optical microscopy showed that there were two types of damage defects. The first kind of damage was a crystal slip, as shown in Fig. 6. The initial image of the specimen is shown in Fig. 6a. The material was composed of ferrite, pearlite, and inclusion. A few slip lines were found at 340 s in the yield stage, as shown in Fig. 6b, but they were not obvious because of the low amplification. The slip lines resulted from high dislocation motion under the applied stress. Q235 steel is a polycrystalline material whose deformation is achieved by the gradual movement of crystals along the slip surface (Zhang *et al.*, 2015). More slip lines were found when the applied load increased or closer to the hardening stage at 514 s, as shown in Fig. 6c. A great number of slip lines appeared in the last necking-fracture stage, as shown in Fig. 6d. A great number of slip lines were also observed for Q235 and 304 steels under tensile test in the plastic stage by Su *et al.* (2018) as shown in Fig. 7.

The other type of damage was an inclusion fracture, as shown in Fig. 8. As shown in Fig. 8b, there was an intact inclusion in the inner part of the crystal initially, while the inclusion fractured suddenly around 291 s during the yield stage Fig. 8c. It should be noted that the specimen was etched in order to improve the quality of the optical micrographs. The erosion possibly leaded to thinning and separation of the inclusion. However, the inclusion was intact at 0 s (Fig. 8b), but it separated into two parts at 291 s (Fig. 8c). What's more, as shown in Fig. 4, there was a burst signal at 291 s. The burst signal meant that higher energy was released. The fracture of inclusion could release higher energy than the crystal slip usually. Therefore, based on the burst signal and the optical micrograph at 291 s, it could deduce that the inclusion fractured due to the tension deformation under the tension load.

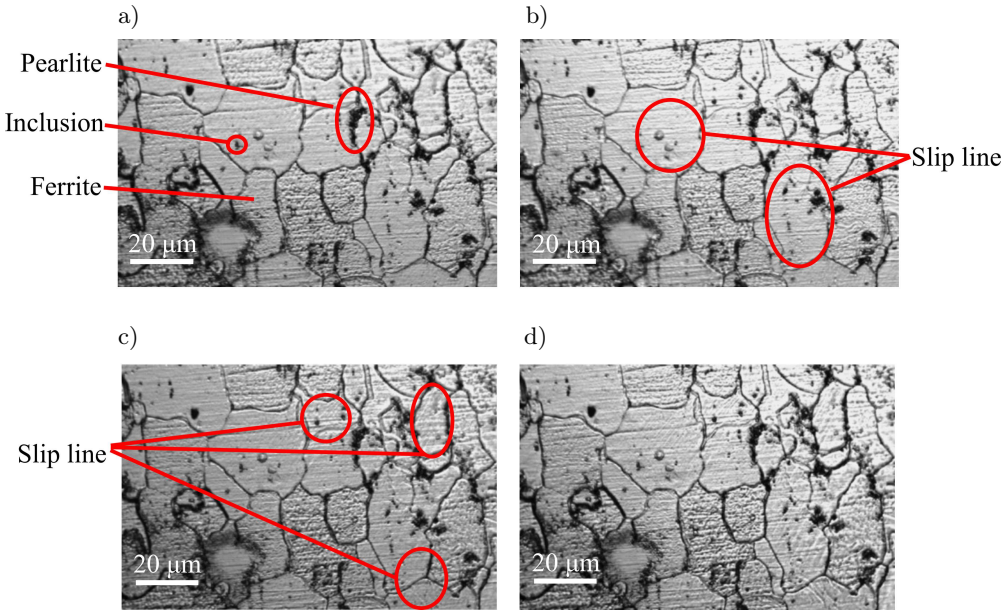

Fig. 6. Optical micrographs of the crystal slip process in Q235 steel: a) 0 s, b) 340 s, c) 514 s, d) 1831 s.

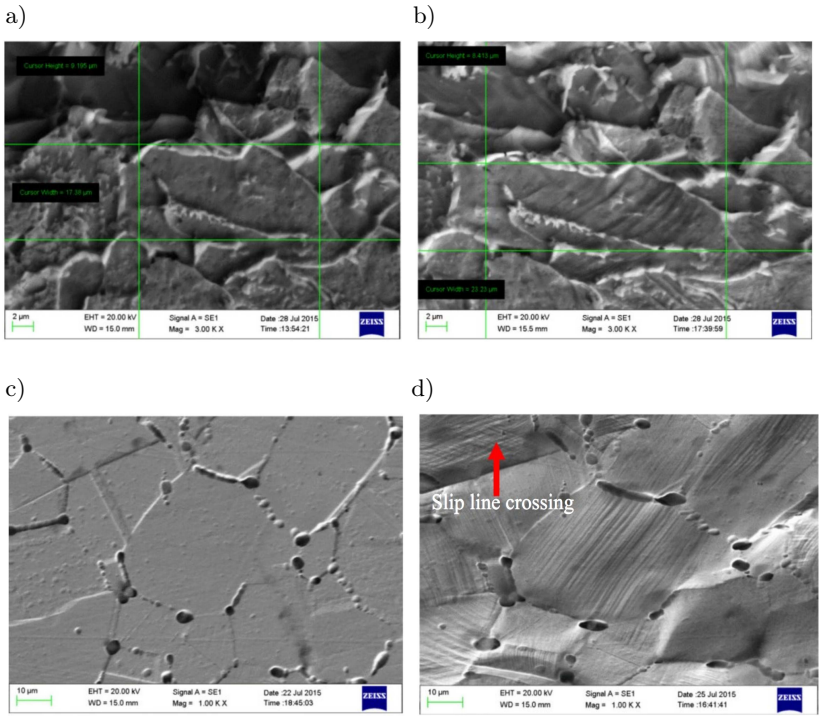

Fig. 7. SEM micrographs of Q235 and 304 steels under tensile test (Su *et al.*, 2018): a) initial morphology of Q235 steel, b) morphology after plastic deformation of Q235 steel, c) initial morphology of 304 steel, d) morphology after plastic deformation of 304 steel.

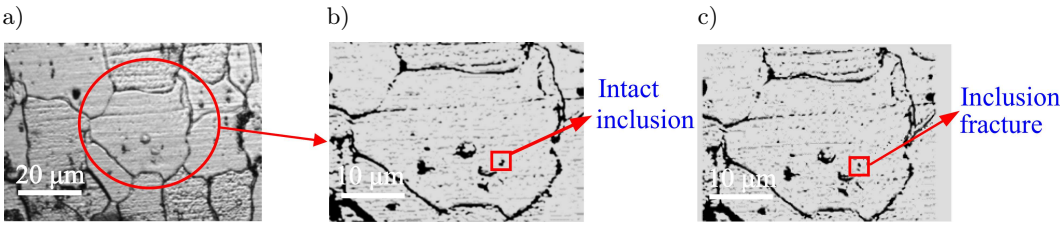

Fig. 8. Optical micrographs of the inclusion fracture process in Q235 steel: a) image at 0 s, b) detailed view at 0 s, c) inclusion fracture at 291 s.

Therefore, the AE signals were generated by the crystal slip and inclusion fracture during the tension deformation. Continuous signals were produced under the ongoing process of the crystal slip. When the inclusion fractured suddenly, a high amount of energy was released rapidly and it possibly led to the bursts of AE signals.

4. Conclusions

In this study, the tension damage process of Q235 steel was investigated using an AE technique and observed by optical microscopy. The main conclusion were:

1) The test results indicate that the damage in Q235 steel was mainly induced by the crystal slip and the inclusion fracture.
2) Both burst and continuous AE signals were observed during the tensile test. The amplitude, the ringing count, and the center frequency of the burst signals were larger than for the continuous signals.
3) A large number of AE signals with high amplitude was generated in the yield stage. Then, their number and amplitude decreased. It was not possible to distinguish the hardening stage and the necking-fracture stage using the amplitude of the AE signals.

Acknowledgments

This study was funded by the National Natural Science Foundation Project of China (51705078), Fundamental Research Funds for the Central Universities (45000-31610029), and Ministry of Industry & Information Technology of China (Z135060009002).

References

1. Bohlen J., Chmelík F., Dobroň, Letzig D., Lukáč P., Kainer K.U. (2004), *Acoustic emission during tensile testing of magnesium AZ alloys*, Journal of Alloys and Compounds, **378**, 214–219, doi: 10.1016/j.jallcom.2003.10.101.
2. Chen Z., Hao X., Wang Y., Zhao K. (2014), *In-situ observation of tensile fracture in A357 casting alloys*, Journal of Materials Science & Technology, **30**, 2, 139–145, doi: 10.1016/j.jmst.2013.04.014.
3. Casiez N., Deschanel S., Monnier T., Lame O. (2014), *Acoustic emission from the initiation of plastic deformation of polyethylenes during tensile tests*, Polymer, **55**, 25, 6561–6568, doi: 10.1016/j.polymer.2014.09.044.
4. Heiple C.R., Carpenter S.H. (1987), *Acoustic emission produced by deformation of metals and alloys – a review, Part I*, Journal of Acoustic Emission, **6**, 3, 177–204.
5. Haidar K., Pijaudier-Cabot G., Dubé J.F., Loukili A. (2005), *Correlation between internal length, fracture, process zone and size effect in mortar and model materials*, Materials and Structures, **38**, 2, 201–210, doi: 10.1007/BF02479345.
6. Ito K., Enoki M. (2007), *Acquisition and analysis of continuous acoustic emission waveform for classification of damage sources in ceramic fiber mat*, Materials Transactions, **48**, 6, 1221–1226, doi: 10.2320/matertrans.I-MRA2007850.
7. Jiang Y., Xu F. (2012), *Research on source location from acoustic emission tomography*, 30th European Conference on Acoustic Emission Testing & 7th International Conference on Acoustic Emission, Granada, Spain.
8. Jiang Y., Xu F., Xu B. (2015), *Acoustic emission tomography based on simultaneous algebraic reconstruction technique to visualize the damage source location in Q235B steel plate*, Mechanical Systems and Signal Processing, **64–65**, 452–464, doi: 10.1016/j.ymssp.2015.04.013.
9. Lugo M., Jordon J.B., Horstemeyer M.F., Tschopp M.A., Harris J., Gokhale A.M. (2011), *Quantification of damage evolution in a 7075 aluminum alloy using an acoustic emission technique*, Materials Science and Engineering A, **528**, 22–23, 6708–6714, doi: 10.1016/j.msea.2011.05.017.
10. Li Z., Limodin N., Tandjaoui A., Quaegebeur P., Witz J., Balloy D. (2016), *Damage investigation in A319 aluminum alloy by digital image correlation during in-situ tensile tests*, Procedia Structural Integrity, **2**, 3415–3422, doi: 10.1016/j.prostr.2016.06.426.
11. Mire E., Carmona V., Courbon J., Ludwig W. (2007), *Fast X-ray tomography and acoustic emission study of damage in metals during continuous tensile tests*, Acta Materialia, **55**, 20, 6806–6815, doi: 10.1016/j.actamat.2007.08.043.
12. Rabiei M., Modarres M. (2013), *Quantitative methods for structural health management using in situ acoustic emission monitoring*, International Journal of Fatigue, **49**, 81–89, doi: 10.1016/j.ijfatigue.2012.12.001.
13. Reuther G.M., Pufall R. Goroll M. (2014), *Acoustic detection of micro-cracks in small electronic devices*, Microelectronics Reliability, **54**, 9–10, 2118–2122, doi: 10.1016/j.microrel.2014.07.129.
14. Shao H., Zhao Y., Ge P., Zeng W. (2013), *In-situ SEM observations of tensile deformation of the lamellar microstructure in TC21 titanium alloy*, Materials Science & Engineering A, **559**, 515–519, doi: 10.1016/j.msea.2012.08.134.
15. Su F., Li T., Pan X., Miao M. (2018), *Acoustic emission responses of three typical metals during plastic and creep deformations*, Experimental Techniques, **42**, 6, 685–691, doi: 10.1007/s40799-018-0274-x.
16. Trojanová Z., Száraz Z., Chmelík F., Lukáč P. (2010), *Acoustic emission from deformed Mg-Y-Nd alloy and this alloy reinforced with SiC particles*, Journal of Alloys and Compounds, **504**, 2, L28–L30, doi: 10.1016/j.jallcom.2010.05.138.

17. Wu Z., Shen G., Wang S. (2008), *The acoustic emission monitoring during the bending test of Q235 steel box beam*, 17th word conference on nondestructive testing, Shanghai, China, pp. 25–28.

18. Xu J., Wu X., Han E. (2011), *Acoustic emission during pitting corrosion of 304 stainless steel*, Corrosion Science, **53**, 4, 1537–1546, doi: 10.1016/j.corsci.2011.01.030.

19. Zhang Y., Zhang W., Xu F., Zhang Y., Jiang Y. (2015), *Acoustic emission characteristics of Q235B steel plates' tensile damage tests* [in Chinese], Journal of Vibration and Shock, **34**, 15, 156–161, 10.13465/j.cnki.jvs.2015.15.028.

20. Zhang K., Ni L., Lei Z., Chen Y., Hu X. (2017), *In situ investigation of the tensile deformation of laser welded Ti2AlNb joints*, Materials Characterization, **123**, 51–57, doi: 10.1016/j.matchar.2016.11.009.

21. Zhang X., Zhang S., Zhao Q., Zhao Y., Li R., Zeng W. (2018), *In-situ observations of the tensile deformation and fracture behavior of a fine-grained titanium alloy sheet*, Journal of Alloys and Compounds, **740**, 660–668, doi: 10.1016/j.jallcom.2018.01.009.